

MIT Open Access Articles

Seagrass blade motion under waves and its impact on wave decay

The MIT Faculty has made this article openly available. **Please share** how this access benefits you. Your story matters.

Citation: Luhar, M. et al. "Seagrass Blade Motion Under Waves and Its Impact on Wave Decay." *Journal of Geophysical Research: Oceans* 122, 5 (May 2017): 3736–3752 © 2017 American Geophysical Union

As Published: <http://dx.doi.org/10.1002/2017JC012731>

Publisher: American Geophysical Union (AGU)

Persistent URL: <http://hdl.handle.net/1721.1/117407>

Version: Original manuscript: author's manuscript prior to formal peer review

Terms of use: Creative Commons Attribution-Noncommercial-Share Alike



1 **Seagrass blade motion under waves and its impact on**
2 **wave decay**

M. Luhar,¹ E. Infantes,² and H. Nepf³

Corresponding author: M. Luhar, Department of Aerospace and Mechanical Engineering, University of Southern California, Los Angeles, CA, USA. (luhar@usc.edu)

¹Department of Aerospace and
Mechanical Engineering, University of
Southern California, Los Angeles,
California, USA

²Department of Marine Sciences,
University of Gothenburg, Gothenburg,
Sweden

³Department of Civil and Environmental
Engineering, Massachusetts Institute of
Technology, Cambridge, Massachusetts,
USA

Key Points.

- Wave decay over a model seagrass bed was measured in experiments that also involved blade motion imaging.
- The reduction in wave energy dissipation due to vegetation motion depends on the Cauchy number.
- Scaling laws developed for individual blades are able to predict the reduction in wave decay over the meadow.

3 **Abstract.** The hydrodynamic drag generated by seagrass meadows can
4 dissipate wave energy, causing wave decay. It is well known that this drag
5 depends on the relative motion between the water and the seagrass blades,
6 yet the impact of blade motion on drag and wave energy dissipation remains
7 to be fully characterized. In this experimental study, we examined the im-
8 pact of blade motion on wave decay by concurrently recording blade posture
9 during a wave cycle and measuring wave decay over a model seagrass meadow.
10 We also identified a scaling law that predicts wave decay over the model meadow
11 for a range of seagrass blade density, wave period, wave height, and water
12 depth scaled from typical field conditions. Blade flexibility led to significantly
13 lower drag and wave decay relative to theoretical predictions for rigid, up-
14 right blades. To quantify the impact of blade motion on wave decay, we em-
15 ployed an effective blade length, l_e , defined as the rigid blade length that leads
16 to equivalent wave energy dissipation. We estimated l_e directly from images
17 of blade motion. Consistent with previous studies, these estimates showed
18 that the effective blade length depends on the dimensionless Cauchy num-
19 ber, which describes the relative magnitude of the wave hydrodynamic drag

20 and the restoring force due to blade rigidity. As the hydrodynamic forcing
21 increases, the blades exhibit greater motion. Greater blade motion leads to
22 smaller relative velocities, reducing drag and wave energy dissipation (i.e.
23 smaller l_e). Imaging-based estimates for l_e agreed well with a scaling law de-
24 rived from a simple force balance for flexible blades moving under wave forc-
25 ing. The same scaling law also led to accurate predictions for wave decay.

1. Introduction

26 Seagrasses are often termed ecosystem engineers because of their ability to alter local
27 hydrodynamic conditions. Because seagrasses are a source of drag, they reduce near-bed
28 water flow, and dissipate current- and wave-energy. In addition to serving as shelter
29 for fauna, the low-flow environment within seagrass beds also leads to reduced sediment
30 resuspension and increased sediment retention [e.g. *Gacia et al.*, 1999; *Duarte et al.*, 1999;
31 *Granata et al.*, 2001]. For example, *Fonseca et al.* [1983] observed that finite patches of
32 seagrass were associated with local maxima in bed elevation in conditions with both
33 current and waves, and attributed this effect to enhanced particle retention within the
34 meadow. In addition to reducing flow locally, regionally the drag generated by seagrasses
35 can lead to significant wave decay [*Fonseca and Cahalan*, 1992]. Smaller waves lead to
36 lower near-bed flows, which could play an important role in reducing shoreline erosion.

37 Wave attenuation by submerged vegetation (including salt marsh vegetation and kelp
38 forests) has been studied in the laboratory [e.g. *Fonseca and Cahalan*, 1992; *Kobayashi*
39 *et al.*, 1993; *Augustin et al.*, 2009; *Sánchez-González et al.*, 2011; *Stratigaki et al.*, 2011;
40 *Paul et al.*, 2012; *Anderson and Smith*, 2014], in the field [e.g. *Knutson et al.*, 1982; *Elwany*
41 *et al.*, 1995; *Mork*, 1996; *Coops et al.*, 1996; *Möller et al.*, 1999; *Bradley and Houser*, 2009;
42 *Riffe et al.*, 2011; *Infantes et al.*, 2012], and using analytical methods or numerical models
43 [e.g. *Kobayashi et al.*, 1993; *Asano et al.*, 1992; *Méndez et al.*, 1999; *Méndez and Losada*,
44 2004; *Peterson et al.*, 2004; *Chen et al.*, 2007]. Most of these studies recognize that it
45 is the relative motion between water and vegetation that sets drag. Yet, a number of
46 these studies ignore the motion of the vegetation, which can lead to large errors in the

47 estimation of wave damping. For example, if the blade tip follows the wave passively, it
48 generates no drag.

49 In their analytical study, [Méndez *et al.*, 1999] accounted for plant motion by imposing a
50 blade excursion that increases linearly with height, and used the resulting relative velocity
51 to calculate drag. In a field study, [Bradley and Houser, 2009] accounted for blade motion
52 by recording the movement of seagrass blade tips from above and, assuming a cantilever
53 model, translated tip excursion into blade motion over the entire blade height. Although
54 blade motion at the top of the meadow was significant in this study, wave decay was still
55 predicted reasonably well with a rigid blade model. Bradley and Houser [2009] attributed
56 this to the fact that the blades were moving in response to a broad wave spectrum, and so
57 the resulting blade motion was out of phase with the peak wave frequency. Other studies
58 [e.g. Méndez and Losada, 2004; Sánchez-González *et al.*, 2011; Infantes *et al.*, 2012] have
59 employed bulk drag or friction coefficients that are calibrated to account for vegetation
60 motion.

61 In recent years, there has been an increasing emphasis on quantifying the effect of
62 vegetation flexibility on bending and motion, and the effect of this bending and motion
63 on wave damping. For example, Mullarney and Henderson [2010] developed an analytical
64 dynamic model for single-stem salt marsh vegetation under wave forcing, assuming that
65 the stems can be modeled using linearized beam theory and that the hydrodynamic forcing
66 is dominated by drag (i.e. inertial effects such as added mass do not play a role). Following
67 on from this study, Riffe *et al.* [2011] measured the dissipation of waves over salt marsh
68 vegetation and found that the rate of dissipation was about half that expected over rigid
69 vegetation. However, the predicted dissipation rates were much closer to the observations

70 when the model developed by *Mullarney and Henderson* [2010] was used to account for
71 vegetation motion.

72 While models based on linear beam theory are reasonable for relative stiff salt marsh
73 vegetation that undergoes limited bending in response to flow, such models may not ap-
74 ply for more flexible vegetation (e.g. seagrass) that experiences substantial bending and
75 motion. With this in mind, *Luhar and Nepf* [2016] developed a more complete numerical
76 model for the wave-induced dynamics of flexible blades that accounts for large deforma-
77 tions as well as inertial effects, and validated this model via laboratory experiments. This
78 study showed that blade motion is governed primarily by two dimensionless parameters:
79 (i) the Cauchy number, Ca , which represents the relative magnitude of the hydrodynamic
80 forcing to the restoring force due to blade stiffness, and (ii) the ratio of blade length to
81 wave orbital excursion, L . For large wave excursions ($L \ll 1$), the flow resembles a uni-
82 directional current and the scaling laws developed in previous steady-flow reconfiguration
83 studies [*Alben et al.*, 2002; *Gosselin et al.*, 2010; *Luhar and Nepf*, 2011] apply. For small
84 excursions ($L \gg 1$), the beam equations may be linearized and the model developed by
85 *Mullarney and Henderson* [2010] holds. Further, *Luhar and Nepf* [2016] showed that the
86 small-excursion scaling laws apply even for intermediate cases with $L \sim O(1)$.

87 The present paper builds on these recent advances in our ability to model wave-
88 vegetation interaction by providing a thorough examination of the effects of blade motion
89 on wave damping. In particular, the laboratory study described below is unique in that
90 it provides detailed observations of blade posture and blade motion over the entire length
91 of the blade for a submerged flexible meadow, designed to mimic the seagrass *Zostera*
92 *marina*, interacting with progressive waves. By observing blade motion over the entire

93 blade length, the experiments offer new insight into the vertical distribution of wave drag
 94 in a meadow and its impact on wave damping. In addition, the stem density, wave period,
 95 amplitude, and water depth are varied systematically over a parameter range compara-
 96 ble to that observed in the field to elucidate the impact of each variable on wave decay.
 97 Broadly, our results show that the dimensionless framework developed by *Luhar and Nepf*
 98 [2016] for individual blades adequately accounts for the effect of blade motion on wave
 99 decay at the canopy-scale. Finally, for field application, we also consider the impact of
 100 submerged vegetation at the regional scale by calculating the ratio of the steady-state
 101 wave heights for wind-generated waves over a vegetated bed relative to a sandy bed.

2. Theory

2.1. Wave Energy Dissipation

102 For the wave decay analysis, we follow the model proposed by *Dalrymple et al.* [1984].
 103 Assuming linear wave theory is valid and that energy dissipation in the seagrass meadow
 104 alone is responsible for wave decay, the steady state energy balance for monochromatic
 105 waves is given by:

$$106 \quad \frac{\partial}{\partial x} \left(\frac{1}{2} \rho g a^2 c_g \right) = -E_D. \quad (1)$$

107 Here, x is the direction of wave propagation, ρ is the density of the water, g is the
 108 acceleration due to gravity, a is the wave amplitude, c_g is the wave group speed, and E_D
 109 is the rate of energy dissipation per unit bed area due to the presence of the vegetation.

110 Using a standard quadratic drag law, E_D can be expressed as:

$$111 \quad E_D = \frac{1}{T} \int_0^T \int_0^l \frac{1}{2} \rho C_D a_v |u_R| u_R u \, dz \, dt. \quad (2)$$

112 The parameter a_v is the vegetation frontal area per unit volume, C_D is the drag coefficient,
 113 u_R is the *relative* horizontal velocity between the vegetation and the water, u is the
 114 absolute water velocity, l is the blade length, and T is the wave period. Note that z
 115 represents the vertical coordinate ($z = 0$ at the bed) and t denotes time.

116 A number of assumptions have been made to yield [2]. Following previous researchers
 117 [*Dalrymple et al.*, 1984; *Méndez and Losada*, 2004; *Bradley and Houser*, 2009], inertial
 118 forces due to the relative acceleration of water and vegetation have been ignored. This is
 119 a reasonable assumption since inertial forces tend to be out of phase with water velocity,
 120 causing little dissipation over a wave cycle. Given the morphology of seagrasses (tall,
 121 thin blades), the vertical drag force is also assumed to be negligible compared to the
 122 horizontal drag force. This assumption breaks down as the blades get pushed over into a
 123 bent posture. We account for this inconsistency below in Section 3.

124 If the wave-induced velocities are adequately described by linear wave theory, the hori-
 125 zontal velocity is:

$$126 \quad u = a\omega \frac{\cosh kz}{\sinh kh} \sin \omega t, \quad (3)$$

127 and the vertical velocity is

$$128 \quad w = a\omega \frac{\sinh kz}{\sinh kh} \cos \omega t. \quad (4)$$

129 Here, $\omega = 2\pi/T$ is the wave radian frequency, $k = 2\pi/\lambda$ is the wavenumber (λ is wave-
 130 length), and h is water depth. The dispersion relation $\omega^2 = kg \tanh(kh)$ describes the
 131 relationship between wave frequency and wavenumber.

132 For rigid vegetation, the relative velocity between the vegetation and the water is iden-
 133 tical to the absolute fluid velocity, $u_R = u$. At this limit, [2] can be integrated and

134 substituted into [1] to yield (assuming C_D and a_v are constant)

$$135 \quad \frac{\partial}{\partial x} \left(\frac{1}{2} \rho g a^2 c_g \right) = -\frac{2}{3\pi} \rho C_D a_v \left(\frac{a\omega}{\sinh kh} \right)^3 \left[\frac{9 \sinh kl + \sinh 3kl}{12k} \right], \quad (5)$$

136 which has a solution of the form

$$137 \quad \frac{a}{a_0} = \frac{1}{1 + K_D a_0 x}. \quad (6)$$

138 Here, a_0 is the initial wave amplitude at $x = 0$ (defined as the start of the meadow) and

139 K_D is a constant, defined as

$$140 \quad K_D = \frac{2ka_v}{9\pi} C_D \left[\frac{9 \sinh kl + \sinh 3kl}{\sinh kh(\sinh 2kh + 2kh)} \right]. \quad (7)$$

141 Note that using a quadratic drag law does not lead to exponential wave decay, which

142 is the fitting model used most frequently for wave decay analyses. However, for small

143 $K_D a_0 x$, the behavior is very similar. Specifically, $\exp(-K_D a_0 x) \approx (1 + K_D a_0 x)^{-1}$ for

144 $K_D a_0 x < 0.5$. Throughout this paper, we use the dimensionless parameter $K_D a_0 \lambda$ to

145 represent wave decay. [This dimensionless parameter can be considered the relative decay](#)

146 [in wave amplitude over a distance equal to the wavelength.](#) From [7], this dimensionless

147 wave decay rate can be expressed as:

$$148 \quad K_D a_0 \lambda = \frac{4a_v a_0}{9} C_D \left[\frac{9 \sinh kl + \sinh 3kl}{\sinh kh(\sinh 2kh + 2kh)} \right]. \quad (8)$$

149 For flexible vegetation that moves in response to flow, the drag force in [2] must be

150 calculated based on the relative velocity. Previous studies have employed simplified can-

151 tilever models (i.e. models based on linear beam theory) for blade motion to estimate

152 relative velocities [*Bradley and Houser, 2009; Mullarney and Henderson, 2010*]. Our ob-

153 servations of blade motion, described below, suggest that a simple cantilever model may

154 not be appropriate under all wave forcing, as the degree of blade curvature far exceeds the

155 assumptions of linear beam theory. To quantify the impact of blade motion on wave de-
156 cay, we employ an effective blade length l_e , which is defined as the rigid blade length that
157 dissipates the same wave energy as the moving flexible blade. Under these assumptions,
158 [5]-[8] remain valid but l is replaced by the effective length l_e . We estimate this effective
159 length directly from blade posture images captured over a wave cycle. This is described
160 in Section 3. The dependence of blade motion, and specifically l_e , on the forces acting on
161 the blade is considered in Section 2.2 below.

162 Finally, by assuming that the fluid velocity over the entire water depth is given by
163 linear wave theory, we ignore the possible reduction of wave-induced velocity within the
164 meadow. *Lowe et al.* [2007] show that wave-induced velocities may be reduced significantly
165 within vegetated canopies if the horizontal wave excursion, A , is much longer than the
166 drag length scale of the vegetation, given by a_v^{-1} . The reduction of wave-induced velocity
167 within the meadow can have a major impact on energy dissipation within the meadow,
168 which is proportional to $|u|u^2$. For the majority of the experimental runs presented in this
169 paper, the wave excursion is shorter than the drag length scale. As a result, the wave-
170 induced velocity is not significantly diminished within the meadow, as shown in *Luhar*
171 *et al.* [2010]. However, we keep this limit in mind when interpreting our experimental
172 results for field application.

2.2. Blade Motion and Effective Length

173 As noted above, to account for the effect of blade motion on drag and wave decay, we
174 employ an effective blade length l_e . *Luhar and Nepf* [2016] show that this effective blade
175 length depends primarily on two dimensionless parameters: (i) the Cauchy number, Ca ,

176 and (ii) the ratio of blade length to wave excursion, L . Here, we provide a brief review of
 177 the scaling laws for effective length identified in *Luhar and Nepf* [2016].

178 The Cauchy number is defined as:

$$179 \quad Ca = \frac{\rho b U^2 l^3}{EI}, \quad (9)$$

180 in which b is the blade width, U is a characteristic wave-velocity scale (assumed to be the
 181 magnitude of u at the bed [3]), E is the elastic modulus of the blade, and $I = bd^3/12$ is
 182 the second moment of area for the blade cross-section, where d is blade thickness. The
 183 length ratio is defined as:

$$184 \quad L = \frac{l}{A} \quad (10)$$

185 where $A = U/\omega$ is the wave orbital excursion.

186 When the drag associated with wave forcing is much smaller than the restoring force due
 187 to stiffness, $Ca \ll 1$, the blade remains upright in the flow. At this effectively-rigid limit,
 188 the hydrodynamic drag generated by the blade is predicted well by assuming a typical
 189 flat plate drag coefficient. However, as the wave forcing increases such that $Ca > O(1)$,
 190 the blade begins to bend and move in response to the wave. The resulting reduction in
 191 drag depends on the length ratio L .

192 At the limit of large wave excursion ($L \ll 1$), we have a quasi-steady situation in
 193 which a flexible blade can be pushed over into a bent posture in the early stages of a
 194 wave half-cycle (see Figure 1a). The blade remains bent until the oscillatory flow reverses
 195 direction. The bent posture held during most of the wave cycle reflects a balance between
 196 the restoring force due to stiffness and the hydrodynamic drag. In this reconfigured state,
 197 the restoring force due to stiffness scales as $EI(\partial^2\theta/\partial s^2) \sim EI(1/l_e^2)$, in which θ is the

198 local blade angle relative to the vertical and s is the distance along the blade (Figure 2).
 199 Similarly, the drag force scales as $F_x \sim \rho b l_e U^2$. In other words, both the blade curvature
 200 and the drag scale depend on the effective length in the reconfigured state. This balance
 201 between stiffness and drag, $EI(1/l_e^2) \sim \rho b l_e U^2$, can be rearranged to yield the following
 202 scaling law:

$$203 \quad \frac{l_e}{l} \sim Ca^{-1/3}. \quad (11)$$

204 This scaling law, first proposed by *Alben et al.* [2002], is identical to that found for
 205 reconfiguration in *steady* flow.

206 At the limit of small wave excursions ($L \gg 1$), we anticipate that the blade remains
 207 nearly vertical as it oscillates back and forth over a wave cycle, and that the horizontal
 208 excursion of the blade scales with the wave excursion (Figure 1b). For this small-deflection
 209 limit, the blade curvature term can be linearized such that $\partial^2\theta/\partial s^2 \approx \partial^3 x_v/\partial z_v^3$, in which
 210 x_v and z_v are the local horizontal and vertical coordinates along the blade (Figure 2).
 211 Since the blade horizontal excursion scales on the wave excursion, $|x_v| \sim A$, balancing
 212 blade stiffness and drag for this small excursion limit yields $EI(A/l_e^3) \sim \rho b l_e U^2$. Using
 213 the definition of Ca and L , this balance can be rewritten as:

$$214 \quad \frac{l_e}{l} \sim (CaL)^{-1/4}. \quad (12)$$

215 With this scaling, the effective length l_e represents the length over which there is significant
 216 relative motion between the blade and the water. The upper part of the blade moves
 217 nearly passively with the flow, contributing negligible drag. Note that this small-deflection
 218 behavior is identical to that described in the analytical model developed by *Mullarney*
 219 *and Henderson* [2010].

220 The scaling laws shown in [11]-[12] both assume that drag is the dominant hydrodynamic
 221 forcing. For wave-induced oscillatory flows, inertial effects such as added mass can also
 222 be important. The drag force per unit blade length is expected to scale as $\rho b U^2$, while
 223 added mass is expected to scale as $\rho b^2 U \omega$ [Vogel, 1994]. Thus, the Keulegan-Carpenter
 224 number, $KC = UT/b$, which represents the ratio of wave orbital excursion to the blade
 225 width [Keulegan and Carpenter, 1956; Graham, 1980], can be used to assess the relative
 226 magnitude of drag and inertial effects. For the conditions tested in the present study,
 227 $KC \geq 11$ (Table 1), and so inertial effects are expected to be less important than drag.

228 Further, the scaling laws also neglect the influence of blade buoyancy. The relative
 229 magnitude of the restoring force due to buoyancy and the restoring force due to stiffness
 230 is denoted by the buoyancy parameter:

$$231 \quad B = \frac{(\rho - \rho_v) g b d l^3}{EI}, \quad (13)$$

232 in which ρ_v is the blade density. Luhar and Nepf [2011] show that for steady flows with
 233 $B \gg 1$, the additional restoring force due to buoyancy can delay the onset of reconfig-
 234 uration. Specifically, the blade does not begin to bend until the hydrodynamic forcing
 235 is large enough to overcome buoyancy, $Ca > O(B)$. However, once the hydrodynamic
 236 forcing exceeds the buoyancy force, $Ca \gg B$, the scaling law shown in [11] applies. For
 237 further discussion on why buoyancy does not alter [11], the reader is referred to Luhar
 238 and Nepf [2011]. Thus, buoyancy could delay the onset of bending for the quasi-steady
 239 large-excursion limit illustrated in Figure 1a without affecting the eventual scaling law
 240 shown in [11]. On the other hand, for the small-deflection limit shown in Figure 1b, buoy-
 241 ancy is unlikely to play a major dynamic role. This is because blade motion is dictated
 242 primarily by the balance of forces acting perpendicular to the blade. At the limit where

243 $L \gg 1$, the blades remain nearly upright and so the effect of buoyancy would only affect
244 the force balance along the blade, i.e. in the vertical direction. For all the laboratory
245 experiments discussed below, $Ca \gg B$ and $L \geq 2.7$ (Table 1). For these high forcing
246 conditions with relatively small wave excursions, we do not expect buoyancy effects to be
247 important.

3. Experimental Methods

248 Laboratory experiments were carried out in a 24 m long, 38 cm wide and 60 cm high wave
249 channel (Figure 3) in the Environmental Fluid Mechanics Laboratory at MIT. Waves were
250 generated at the upstream end of the channel by a vertical paddle driven by a hydraulic
251 piston. The motion of the paddle was controlled by a Syscomp WGM-101 arbitrary
252 waveform generator programmed to produce surface waves of a desired frequency and
253 amplitude, based on the closed form solution developed by *Madsen* [1971]. A plywood
254 beach with layers of rubberized coconut fiber was installed on the downstream end of the
255 channel. The beach reflected less than 10% of the wave energy.

256 The model seagrass meadow was constructed using artificial plants (Figure 4) [that are](#)
257 [geometrically and dynamically similar to seagrass such as *Zostera marina* \(eelgrass\) and](#)
258 [Posidonia oceanica](#), as described by *Ghisalberti and Nepf* [2002]. Each shoot consisted of
259 a 2.0 cm long basal stem (made from a circular cylinder) and six blades. The blades were
260 attached to the basal stem using a rubber band, which locally increased the diameter. The
261 extent of the overlap between the stem and the blades was 1.0 cm. The stem diameter,
262 d_s , will be defined as the average between the minimum (6.4mm) and maximum (9.2 mm)
263 measured diameters of a typical stem, i.e. $d_s = 7.8$ mm. The blades were cut from low-
264 density ($\rho_v = 920 \text{ kgm}^{-3}$) polyethylene film with a modulus of elasticity, $E = 3.0 \times 10^8$

265 Pa. The blades were $l = 13$ cm long (excluding 1 cm stem overlap), $b = 3$ mm wide, and
 266 $d = 0.1$ mm thick. The buoyancy parameter [13] for these blades is $B = 6.9$.

267 A random algorithm was used to place the stems in pre-drilled baseboards at stem
 268 densities ranging from 300 to 1800 stems m^{-2} (blade densities, $n = 1800 - 10800$ m^{-2}).
 269 Only the top 1.0 cm of the stems, the region attached to the blades, protruded above the
 270 baseboards. The blade density was chosen based on field observations of *Zostera marina*
 271 and *Posidonia oceanica* [Moore, 2004; Marbà et al., 2005; Luhar et al., 2010]. The frontal
 272 area per unit volume for the blades, $a_v = nb$, ranged from 0.054 cm^{-1} to 0.32 cm^{-1} . These
 273 densities correspond to a blade frontal area index $a_v l \approx 0.7$ to 4.2 . Field meadows for
 274 eelgrass have been observed in the range $a_v l \approx 0.3 - 1.1$, based on biomass data from
 275 Moore [2004], converted to frontal area index in Luhar et al. [2008]. For species such as
 276 *Posidonia oceanica*, the frontal area index can be as high as $a_v l \approx 4$ [based on data from
 277 Pergent-Martini et al., 1994].

278 To achieve similarity in wave conditions, the following dimensionless parameters were
 279 matched to field conditions: kh (the ratio of wavelength to water depth), and l/h (blade
 280 length to water depth). Most seagrass species ($> 75\%$) are found in less than 20 m depth
 281 [Duarte, 1991] and are affected by wave peak periods from 0.6 to 15 s [Ward et al., 1984;
 282 Koch et al., 2006; Bradley and Houser, 2009]. Based on these conditions, we chose values
 283 of kh ranging from 0.6 to 2.7 and l/h ranging from 0.3 to 0.8, which represent the shallow
 284 region of a seagrass meadow. For example, assuming blades of length $l \approx 1$ m [Luhar et al.,
 285 2013; Eriander et al., 2016], $kh = 0.6$ and $l/h = 0.3$ correspond approximately to waves
 286 of period 6s in 3m water depth; $kh = 2.7$ corresponds approximately to waves of period
 287 $T = 2$ s. Similarly, the typical amplitude ratio employed in the experiments (Figure 3),

288 $a_0/h \approx 0.1$ scales to waves of amplitude 30 cm in 3 m water depth. The length of the
289 model meadow, 500 cm, was 1.4 to 5.5 times the wavelength λ . The leading edge of the
290 meadow is denoted $x = 0$.

291 The wave parameters for each individual experiment are listed in Table 1. For reference,
292 the wave period ranged from $T = 0.8$ s to 2.0 s (Runs T1-T5), the wave amplitude
293 upstream of the meadow ranged from $a_0 = 0.9$ cm to 5.6 cm (Runs A1-A5), and the
294 water depth ranged from $h = 16$ cm to 39 cm (Runs H1-H4). Table 1 also lists the
295 Reynolds number based on blade width ($Re = Ub/\nu = 100 - 610$, where ν is the kinematic
296 viscosity of water), the Keulegan-Carpenter number ($KC = 11 - 102$), the Cauchy number
297 ($Ca = 100 - 3610$), and ratio of blade length to wave excursion ($L = 2.7 - 25.9$) for each
298 case.

299 The wave amplitude was measured using two resistance-type wave gauges with 0.2
300 mm accuracy. One wave gauge was permanently mounted at $x = 125$ cm to provide a
301 reference measurement verifying that the wave conditions were constant throughout the
302 experimental run. The second wave gauge was mounted on a mobile trolley that moved
303 on precision rails. The mobile gauge was used to measure wave records at 20 cm intervals
304 from 40 cm upstream of the meadow and continuing along its entire length. At each
305 x position, the instantaneous position of the water surface was measured at 25 Hz for
306 120 seconds (60-132 waves, depending on wave frequency). The surface displacement
307 measurements were binned into $25T$ phase groups (e.g. 50 phase groups for waves of
308 period $T = 2.0$ s) based on the zero-crossings of the record, and averaged, yielding a
309 phase-averaged waveform $\eta(t)$. The wave amplitude was calculated based on the root

310 mean squared value of the phase-averaged waveform:

$$311 \quad a = \sqrt{\frac{2}{T} \int_0^T \eta^2(t) dt}. \quad (14)$$

312 Equation [6] was then fitted to the wave amplitude measurements to obtain the decay
 313 parameter $K_D a_0 \lambda$ for each experiment. As an example, the measured wave amplitudes
 314 and fitted decay curves for runs H1 ($a_0 = 1.4$ cm, $T = 1.4$ s, $h = 16$ cm, see Table 1)
 315 and T5 ($a_0 = 3.5$ cm, $T = 2.0$ s, $h = 39$ cm) are shown in Figure 5. The major source
 316 of error for the wave decay fits was the partially standing wave created in the flume
 317 because of reflections ($< 10\%$) from the downstream end. Due to this standing wave,
 318 the measured wave amplitude exhibited small oscillations, periodic at a spatial scale of
 319 half the wavelength (Figure 5). Note that wave energy is also dissipated in the laminar
 320 boundary layers at the flume bed and sidewalls due to viscosity. To correct for this, we
 321 subtracted the theoretical viscous decay per wavelength [*Hunt, 1964*] from the fitted decay
 322 parameter. This correction typically resulted in a relative reduction of less than 10% for
 323 the fitted value of $K_D a_0 \lambda$.

324 Blade motion was recorded in images taken midway along the meadow at 15 Hz using
 325 a Sony DFW-X710 CCD camera. Images were taken for the wave conditions marked
 326 with an asterisk in Table 1, but with a lower density ($n = 1800$ blades m^{-2}) for better
 327 image clarity. One of the blades was marked with a red dot at 2 cm intervals along
 328 the blade and the marks were tracked over 5 wave cycles. Neighboring blades moved
 329 in near-unison, hence tracking a single blade was sufficient to characterize blade motion
 330 (see movies in [Supplementary Information](#)). A fifth order polynomial fit to the marked
 331 positions was used to estimate the blade position and angle to the vertical (x_v , z_v , and
 332 θ in Figure 2) as a function of distance along the blade, s , at different phases in the

333 wave cycle. Sinusoidal curves were fitted to the observed blade positions over a wave
 334 cycle to obtain the horizontal and vertical blade velocities ($\partial x_v/\partial t$, $\partial z_v/\partial t$). At higher
 335 stem densities, there was some interference between neighboring blades for certain wave
 336 conditions. The nature of this interference and potential implications for blade motion
 337 tracking are discussed in Section 4.1 below.

338 The observed blade velocities were used together with the horizontal [3] and vertical
 339 [4] orbital velocities predicted by linear wave theory to calculate relative velocities, $u_R =$
 340 $u - (\partial x_v/\partial t)$ and $w_R = w - (\partial z_v/\partial t)$. For all the wave conditions considered in this
 341 study, vertical profiles of velocity measured upstream of the meadow were within 95%
 342 of predictions made by linear theory [Luhar et al., 2010]. The rate of energy dissipation
 343 within the meadow was then estimated using the equation:

$$344 \quad E_D = \frac{1}{T} \int_0^T \int_0^l \frac{1}{2} \rho C_D a_v |u_{RN}| u_{RN} u_N ds dt. \quad (15)$$

345 where $u_{RN} = u_R \cos \theta - w_R \sin \theta$ is the relative velocity normal to the blade, and $u_N =$
 346 $u \cos \theta - w \sin \theta$ is the fluid velocity normal to the blade. As shown in Figure 2, θ is the
 347 angle of the blade relative to vertical, and so [15] accounts for the bent posture of the
 348 blades by considering both horizontal and vertical relative velocities. To estimate the
 349 effective blade length, the rate of energy dissipation calculated using [15] was equated
 350 with the expression shown on the right-hand side of equation [5], replacing l with l_e in
 351 equation [5]. This method of estimating the effective blade length requires the further
 352 assumptions that C_D and a_v are constant in time and in position along the blade, so that
 353 the factor $C_D a_v$ cancels when equating [5] and [15]. Note that in the limit of rigid, upright
 354 vegetation ($\theta = 0$, $u_{RN} = u_R = u$), [15] is identical to the expression shown in [2].

4. Results

4.1. Blade Posture and Motion

355 Movies of blade motion showed behavior that followed or fell between the two cases
356 illustrated in Figure 6. This figure shows the fitted blade posture at six equally spaced
357 phases of a wave cycle for wave conditions corresponding to the lowest amplitude case A1
358 ($a_0 = 0.9$ cm, $T = 1.4$ s, $h = 39$ cm) and the highest amplitude case A5 ($a_0 = 5.6$ cm,
359 $T = 1.4$ s, $h = 39$ cm). Curves marked 1, 2 and 3 show blade posture under the wave
360 crest (forward stroke) while curves 4, 5 and 6 show motion under the wave trough (return
361 stroke). For both runs, the horizontal excursion of the blade tips was comparable to the
362 wave excursion. However, blade motion under the return stroke varied dramatically for
363 the two cases.

364 For the wave conditions in run A1, the blade remained relatively upright as it moved
365 throughout the wave cycle (Figure 6a). For this case, the effective blade length was
366 estimated to be $l_e/l = 0.40$, indicating that blade flexibility significantly reduced the drag
367 (cutting it by more than half) relative to a rigid blade of comparable length. For high
368 amplitude wave conditions, the blade motion was more complex, with significant blade
369 motion over most of the blade length (e.g. run A5, Figure 6b). The blade remained
370 relatively still and upright only very close to the bed. Greater blade motion translated
371 into smaller relative velocities, which led to a further reduction in the effective blade
372 length relative to run A1, specifically the effective length was estimated to be $l_e/l = 0.21$.
373 Photographs from *Koch et al.* [2006] show blade postures in the field similar to those
374 in Figure 6b, confirming the dynamic similarity between natural seagrass and the model

375 employed for this study. Note that *Paul et al.* [2012] also observe broadly similar blade
376 motion in their laboratory experiments.

377 We observed a net mass transport (unidirectional current) in the direction of wave
378 propagation that extended vertically over the height of the seagrass meadow. This induced
379 current is analogous to the steady streaming observed in wave boundary layers [for further
380 detail, see *Luhar et al.*, 2010, 2013]. The magnitude of this steady streaming was large
381 enough (as much as 8 cm s^{-1}) to create a bias in blade posture in the streamwise direction
382 (Figure 6). However, the effective blade length calculated using [15] accounts for this bias
383 in posture¹.

384 For the wave conditions in the intermediate amplitude case A3 ($a_0 = 3.4 \text{ cm}$, $T = 1.4$
385 s, $h = 39 \text{ cm}$), and the low frequency case T5 ($a_0 = 3.5 \text{ cm}$, $T = 2.0 \text{ s}$, $h = 39 \text{ cm}$), blade
386 motion resembled the observed behavior for run A5 (high amplitude, Figure 6b). Blade
387 motion for the high frequency waves in experiment T2 ($a_0 = 2.7 \text{ cm}$, $T = 0.9 \text{ s}$, $h = 39$
388 cm) was similar to that observed for A1 (low amplitude, Figure 6a). The difference in
389 blade motion is reflected in the effective blade lengths reported in Table 1. Note that the
390 wave velocities were larger for experiments A3, A5 and T5 compared to experiments A1
391 and T2, suggesting that hydrodynamic forcing dictates blade motion and sets the effective
392 length, with higher wave-induced velocities leading to smaller effective blade lengths. The
393 relationship between effective length and hydrodynamic forcing is considered in greater
394 detail in Section 5.1.

395 The above image analysis was carried out for blade density $n = 1800 \text{ blades m}^{-2}$.
396 At higher stem density the reduced center-center spacing between the model plants led
397 to interference between neighboring blades. Qualitative observations indicate that blade

398 motion for high frequency or low amplitude waves did not change significantly. The
 399 relatively upright posture of the blades during these runs, similar to Figure 6a, ensured
 400 that there was little interference from neighboring blades. However, the complex blade
 401 motion seen for high amplitude waves (Figure 6b) was affected. At densities above 7200
 402 blades m^{-2} , the upper portions of the blades remained depressed in a streamwise posture
 403 throughout the wave cycle. The blades oscillated periodically between the postures shown
 404 by curves 4, 5 and 6 in Figure 6b, without undergoing the postures shown by curves 1,
 405 2 and 3. This streamwise posture ensures that the upper portions of the blades provide
 406 very little flow resistance (only skin friction). Drag generation is again dominated by the
 407 lower part of the blades and hence, our earlier estimates of effective blade length remain
 408 valid.

4.2. Wave Decay

409 The measured wave decay, expressed as $K_D a_0 \lambda$, is shown in Figure 7 as a function of
 410 the dimensionless vegetation parameters $a_v l$, a_0/h , l/h , and kh . For reference, we also
 411 show curves (black lines in Figure 7) corresponding to the wave decay predicted for rigid,
 412 right blades, i.e. $l_e = l$ in [8]. For simplicity, we assume a constant value for the drag
 413 coefficient for these predictions: $C_D = 1.95$, which corresponds to a flat plate normal to
 414 flow at high Reynolds number.

415 In general, the drag coefficient is expected to vary both as a function of the Reynolds
 416 number, Re , and the Keulegan-Carpenter number, KC . For steady flows, the Reynolds
 417 number dependence can be approximated as $C_D \approx 1.95 + 50/Re$ [Ellington, 1991; Vogel,
 418 1994]. For oscillatory flows at high Reynolds number, *Luhar and Nepf* [2016] suggested
 419 the following dependence $C_D = \max(1.95, 10KC^{-1/3})$ based on data from *Graham* [1980].

420 In the present experiments, the Keulegan-Carpenter number ranged from $KC = 11$ to
 421 102, while the Reynolds number ranged from $Re = 100$ to 610 (Table 1). Based on the ex-
 422 pressions given above, $C_D \approx 2.1 - 4.6$ over this parameter range. Thus, $C_D = 1.95$ is likely
 423 to be an underestimate of the true drag coefficient, making the solid curves in Figure 7
 424 an underestimate of the rigid blade wave dissipation. Despite this **underestimation**, with
 425 the rigid blade assumption, [8] over-predicts wave decay for all the experimental runs,
 426 clearly showing that blade flexibility leads to reduced drag. Significantly, the rigid blade
 427 assumption over-predicts wave decay by a factor of more than 3 in most cases (Figure 7).
 428 Exceptions to this are the high frequency cases, T1 and T2 shown in Figure 7c, and the
 429 low amplitude cases, A1 and A2, shown in Figure 7b. For these cases, the rigid, upright
 430 blade assumption over-predicts wave decay by a factor of 2 to 3, consistent **with** the es-
 431 timated effective blade lengths for runs T2 and A1 ($l_e/l \approx 0.4$, see Table 1). Further,
 432 the over prediction of wave decay by the rigid blade assumption increases with increas-
 433 ing wave amplitude (Figure 7b) and decreasing wave number (Figure 7c), which would
 434 correspond to increasing wave length and period. In other words, the wave decay mea-
 435 surements suggest that an increase in orbital velocity, associated with a higher amplitude
 436 or longer period, leads to a decrease in effective blade length, consistent with the direct
 437 observations of blade posture and motion (Figure 6).

438 In addition to the drag reduction associated with flexible blades presented above, we
 439 also observed the following general trends in wave decay. Wave decay increased with
 440 vegetation density (Figure 7a), and the trend was approximately linear for the lower
 441 vegetation densities. However, wave decay reached a plateau for the two highest densities,
 442 Runs D5 ($n = 9000$ blades m^{-2}) and D6 ($n = 10800$ blades m^{-2}) shown in Figure 7a.

443 Lower decay may be explained based on the arguments put forth by *Lowe et al.* [2007].
 444 As the orbital excursion approaches or exceeds the drag length scale ($A \sim a_v^{-1}$), the wave
 445 induced flow within the meadow is damped, resulting in lower velocities. Lower in-canopy
 446 velocities lead to reduced energy dissipation [2] and wave decay. For run D5 the orbital
 447 excursion was $A = 2.7$ cm, and the drag length scale was $a_v^{-1} = 3.7$ cm, suggesting
 448 that the velocity damping limit was approached ($Aa_v = 0.7$ for D5 and $Aa_v = 0.8$ for
 449 D6). Thus, even though more drag elements were present in case D6, relative to case
 450 D5, the lower in-canopy velocity could produce comparable wave decay. We also expect
 451 diminished wave velocities within the meadow for the following cases: T5 ($Aa_v = 1.1$), A4
 452 ($Aa_v = 0.9$) and A5 ($Aa_v = 1.0$). Velocity measurements reported in *Luhar et al.* [2010]
 453 for these wave conditions show that orbital velocities within the meadow are reduced by
 454 as much as 21% compared to predictions made by linear wave theory.

455 Figure 7c shows the variation in wave decay over a range of wave periods (and also
 456 wavelengths). In general, decay decreased as the waves became shorter (period T de-
 457 creases, kh increases). The decay per wavelength, $K_D a_0 \lambda$, was 0.11 (interpreted as an
 458 11% reduction in wave height per wavelength) for waves of period 2.0 seconds (run T5)
 459 and only $K_D a_0 \lambda = 0.01$ for waves of period 0.8 seconds (run T1). This is physically
 460 intuitive since shorter waves have velocities that decrease more rapidly with depth and
 461 smaller velocities within the meadow lead to reduced energy dissipation and wave decay.
 462 For example, linear wave theory [3]-[4] predicts that a wave of amplitude 5.0 cm in 39
 463 cm water depth would produce a horizontal orbital velocity of 22 cms^{-1} near the flume
 464 bed ($z = 0$ cm) for waves of period $T = 2.0$ s and only 5.6 cms^{-1} for waves of period
 465 0.8 s. Similarly, because velocity increases linearly with amplitude, we also expect higher

466 wave decay for high amplitude waves. This is confirmed by the wave decay measurements
 467 shown in Figure 7b. However, in both Figure 7b and Figure 7c, the observed increase in
 468 wave decay with wave amplitude and period is not as steep as that predicted for rigid,
 469 upright blades. This may be explained by a decrease in effective blade length caused by
 470 higher velocities (and hence higher Cauchy number).

471 Finally, Figure 7d elucidates the impact of relative submergence. The water depth was
 472 varied between 16 cm (H1, $l/h = 0.8$) and 39 cm (H4, $l/h = 0.3$) while the wave period
 473 ($T = 1.4$ s) was kept constant for these runs. As a result, the parameters kh and l/h
 474 both varied for these experiments. The decay per wavelength, $K_D a_0 \lambda$, was 0.25 for case
 475 H1 with $l/h = 0.8$. This reduced to $K_D a_0 \lambda = 0.09$ for the case where $l/h = 0.3$ (H4).
 476 In general, wave decay increased as the meadow occupied more of the water column [see
 477 also *Stratigaki et al.*, 2011; *Anderson and Smith*, 2014]. The predicted curve shown in
 478 Figure 7d suggests that decay is likely to be negligible if the meadow occupies less than
 479 10% of the water column.

5. Discussion

5.1. Effective Length and Wave Decay

480 Figure 7 shows that the rigid blade assumption substantially over-predicts wave decay
 481 over the model canopy of flexible seagrass. Instead of calibrating the drag coefficient to
 482 account for the effect of vegetation motion, we propose the use of the physically-motivated
 483 effective length framework. For the present experiments, the ratio of blade length to wave
 484 excursion was $L \geq 2.7$ and the Cauchy number was $Ca \geq 100$. Thus, we expect the high-
 485 forcing ($Ca \gg 1$) and small-excursion ($L \gg 1$) limit identified by *Luhar and Nepf* [2016]
 486 to apply. For this limit, the effective length is predicted to scale as $l_e/l \sim (CaL)^{-1/4}$ [12].

487 As shown in Figure 8, the effective lengths estimated from blade motion imaging conform
 488 well to this predicted scaling law². More specifically, the following relationship provides
 489 the best fit to the data: $l_e/l = 2.25(CaL)^{-1/4}$ ($r^2 = 0.67$). Importantly, this scaling law is
 490 also consistent with the single blade data reported in *Luhar and Nepf* [2016], which were
 491 obtained via direct force measurements.

492 We next test whether the relation for effective length determined through video analysis
 493 of blade motion (Figure 8) can be used in [8] to predict observed wave decay. Figure 9
 494 compares measured values for wave decay, $K_D a_0 \lambda$, with predictions made via [8]. With
 495 the rigid blade assumption, $l_e = l$, the slope for the best-fit linear relationship between
 496 predicted and measured wave decay is 4.50 (Figure 9a). In other words, the rigid blade
 497 assumption on average leads to a 350% over-prediction of wave decay. Figure 9b shows
 498 that the predictions improve markedly when the effective blade length is calculated using
 499 the fitted relationship, $l_e/l = 2.25(CaL)^{-1/4}$. Specifically, the slope for the best-fit linear
 500 relationship is 1.08, i.e. an 8% over-prediction on average. For most of the cases, the ob-
 501 served values are within 20% of the predictions, which further confirms that our physically
 502 based model for effective length captures the behavior of the model seagrass blades well.
 503 There is one exception to the good prediction provided by the effective length. Specifi-
 504 cally, wave decay is over-predicted substantially for run T5. As discussed above, for this
 505 case the wave excursion exceeds the drag length-scale ($Aa_v = 1.1$), resulting in a reduction
 506 of in-canopy velocities [*Luhar et al.*, 2010] which is not accounted for in equation [8].

507 The results presented in Figure 9 show that the effective length framework successfully
 508 accounts for the effects of blade flexibility on wave energy dissipation, providing an accu-
 509 rate prediction of measured wave decay. A major advantage of this approach is that it

510 allows us to differentiate between the distinct physical phenomena that affect drag and
511 energy dissipation. Specifically, the effects of shape and Reynolds number can be incor-
512 porated into the drag coefficient, so that C_D can be estimated from previous literature for
513 rigid bluff body flows. The effects of vegetation bending and motion can be accounted for
514 via the effective length l_e , which depends primarily on the Cauchy number Ca and length
515 ratio L .

516 For field conditions, the Cauchy number Ca can be calculated based on estimates of
517 the blade properties (width, length, thickness and elastic modulus) and the significant
518 wave height and peak period. However, the exact power law for l_e obtained here may not
519 apply across all species of seagrass. [The broadband nature of waves in the field also makes](#)
520 [defining an effective length more difficult.](#) Specifically, there could be multiple energetic
521 [wave frequencies in the field, and the vegetation is unlikely to dissipate all these frequencies](#)
522 [equally, i.e. the canopy may act as a high- or low-pass filter for the waves \[Bradley and](#)
523 [Houser, 2009\].](#) A single value for l_e identified from the significant wave height and peak
524 [period would not reproduce this frequency dependence, and so it may be necessary to](#)
525 [define a frequency-dependent effective length \[see also Mullarney and Henderson, 2010\].](#)

5.2. Vegetation Effects at the Regional Scale

526 Previous studies [*Gacia et al., 1999; Granata et al., 2001*] suggest that the reduction in
527 wave-induced velocities within seagrass meadows results in lower local bed-stresses. Lower
528 bed stresses lead to reduced sediment re-suspension and, therefore, enhanced particle
529 retention. On a regional scale, the presence of seagrass can also impact the bed stresses
530 by reducing the wave amplitude. We follow the methodology of [*Fagherazzi et al., 2006*] to
531 predict the reduction in wave amplitude over a vegetated region relative to a bare bed and

532 hence, estimate the regional effects on near-bed velocity. We consider locally-generated
 533 wind waves at equilibrium, such that the energy input from the wind is balanced by the
 534 energy extracted by bed friction in the absence of vegetation [as considered by *Fagherazzi*
 535 *et al.*, 2006], or by vegetative drag (as we now consider in comparison). For simplicity, we
 536 ignore energy losses associated with wave breaking and white capping, and we also ignore
 537 the influence of fetch, i.e. we consider an unlimited fetch. The dissipation rate due to bed
 538 friction is:

$$539 \quad E_{D,bf} = 2\rho g C_{bf} a_{bf}^3 \omega \frac{k}{\sinh kh \sinh 2kh} \quad (16)$$

540 with bed friction coefficient, $C_{bf} = 0.015$ [*Fagherazzi et al.*, 2006]. For conditions with
 541 only bed friction (bf) acting, we denote wave amplitude a_{bf} . Wave dissipation due to a
 542 seagrass meadow (repeated here for convenience) is as shown in [5]

$$543 \quad E_{D,veg} = \frac{2}{3\pi} \rho C_D a_v \left(\frac{a_{veg} \omega}{\sinh kh} \right)^3 \left[\frac{9 \sinh kl_e + \sinh 3kl_e}{12k} \right]. \quad (17)$$

544 Here, for conditions with vegetation we denote the wave amplitude as a_{veg} . Since we
 545 compare conditions at the same site, with and without seagrass, the wind-input is the
 546 same. Therefore, we equate [16] and [17], and solve for the ratio a_{veg}/a_{bf} to compare the
 547 amplitude of waves in this region with and without vegetation. This ratio is given by the
 548 expression:

$$549 \quad \left(\frac{a_{veg}}{a_{bf}} \right)^3 = \frac{3\pi}{2} \frac{C_{bf}}{C_D a_v l_e} \left[\frac{12kl_e}{9 \sinh kl_e + \sinh 3kl_e} \right]. \quad (18)$$

550 We compute this amplitude ratio for a typical seagrass meadow [see e.g. *Luhar et al.*,
 551 2010] subject to waves of period $T = 2.0$ s and $T = 8.0$ s. We assume that the seagrass
 552 blade length is $l = 0.5$ m, the water depth ranges from $h = 1$ m to $h = 10$ m, and the
 553 frontal area per unit volume ranges from $a_v = 1$ m⁻¹ to $a_v = 10$ m⁻¹. Since the effective

length depends on the local hydrodynamic forcing, it cannot be predicted independently of the wave amplitude a_{veg} . For simplicity, we assume a constant value of $l_e/l = 0.2$ such that $l_e = 0.1$ m. The drag coefficient is assumed to be $C_D = 1.95$.

As expected, the influence of seagrass on wave amplitude increases as vegetation density (a_v) increases (Figure 10). Recall from Figure 7 that wave decay increases as the fraction of the water column occupied by the vegetation increases (runs H4-H1) and decreases as the wave period decreases (runs T5-T1). However, Figure 10 shows that neither the wave period nor the water depth appreciably impact the amplitude ratio, a_{veg}/a_{bf} . This is because, for field conditions, the effective length of the vegetation is likely to be much smaller than the wavelength, $kl_e = 2\pi l_e/\lambda \ll 1$, and so the factor inside the square brackets in [18] is approximately equal to 1. At this limit, [18] simplifies to:

$$\frac{a_{veg}}{a_{bf}} \approx \left(\frac{2\pi}{2} \frac{C_{bf}}{C_D a_v l_e} \right)^{1/3}. \quad (19)$$

In other words, the wave period, wavelength, and water depth do not play a significant role. Instead, the parameter $C_{bf}/(C_D a_v l_e)$, which may be thought of as the ratio of energy dissipation over the two substrates, is the major control on the amplitude ratio.

Figure 10 shows that, for typical field conditions, the wave amplitude over a meadow is less than 70% of the amplitude over bare bed, i.e. a reduction of 30% or more. For dense meadows ($a_v \approx 10 \text{ m}^{-1}$), the reduction in amplitude can be as large as 70%. Since wave-velocity scales linearly with wave amplitude, a similar reduction in near-bed velocity is expected. Thus, on a regional scale, wave decay due to seagrass meadows is likely to yield a significant reduction of near-bed velocities compared to regions without vegetation. Lower velocities lead to lower bed stresses, thereby reducing sediment re-suspension.

6. Conclusion

576 Through flume experiments, we have studied blade motion under waves and its impact
577 on wave energy dissipation over a seagrass meadow. Only relative motion between the
578 blades and the water leads to hydrodynamic drag and hence, energy dissipation. As a
579 result, the effective length of the seagrass blades, which approximates the length of blade
580 over which relative motion between blades and water is significant, produces a better
581 predictor of energy dissipation than models based on the full blade length. Consistent
582 with recent experimental and theoretical research on the dynamics of flexible blades in
583 oscillatory flows [Mullarney and Henderson, 2010; Luhar and Nepf, 2016], our results
584 suggest that the effective blade length depends on the ratio of the restoring force due
585 to blade rigidity and hydrodynamic drag (Cauchy number, Ca) as well as the ratio of
586 blade length to wave excursion (L). Specifically, the ratio CaL provides a metric for
587 predicting the effective blade length, l_e . The best fit to the data was a power law of
588 the form $l_e/l = 2.25(CaL)^{-1/4}$. Using this estimator of the effective blade length, which
589 was based on images of blade motion, we were able to predict the wave decay over the
590 meadow. Previous researchers have simply used a calibrated value of the drag coefficient
591 to account for blade motion. By studying the posture of the blades over a wave cycle, we
592 give a mechanistic explanation for the lower drag coefficients.

593 We also studied the impact of vegetation characteristics (stem density and depth of sub-
594 mergence) and wave properties (period and amplitude) on wave decay. As anticipated,
595 wave decay increases with increasing vegetation density (more drag-inducing elements).
596 Relative depth of submergence also plays a major role; wave decay increases as the veg-
597 etation occupies a larger fraction of the water column. Further, wave decay decreases

598 with decreasing wave period and increases with increasing wave height. This is because
599 wave-induced velocities within the meadow increase as the wave period and wave height
600 rise, and larger velocities lead to greater energy dissipation within the meadow. Finally,
601 we show that on a regional scale, the amplitudes of steady-state wind-generated waves
602 over seagrass meadows could be less than 40% of the amplitudes over regions without
603 vegetation because of energy dissipation due to vegetation drag.

604 **Acknowledgments.** This study received support from the US National Science Foun-
605 dation under grants OCE 0751358 and [EAR 6935738](#). Any conclusions or recommenda-
606 tions expressed in this material are those of the author(s) and do not necessarily reflect
607 the views of the National Science Foundation. E. Infantes would like to thank financial
608 support from the Spanish Ministerio de Educación y Ciencia (MEC) FPI scholarship pro-
609 gram (BES-2006-12850). All data necessary to evaluate and build upon the work in this
610 paper are available in the cited references, or are included in the figures and tables.

Notes

1. Biased blade postures have also been observed for single blades in oscillatory flows, though the exact mechanisms leading
611 to this mean pronation remain to be fully understood [*Gijón Mancheño, 2016; Luhar and Nepf, 2016*].
2. We also considered the large-excursion scaling, $l_e/l \sim Ca^{-1/3}$, shown in [11]. However, this scaling did not lead to as
good of a fit for the effective lengths, which is understandable given that it assumes $L \ll 1$.

References

- 612 Alben, S., M. Shelley, and J. Zhang (2002), Drag reduction through self-similar bending
613 of a flexible body, *Nature*, *420*(6915), 479–481.
- 614 Anderson, M. E., and J. Smith (2014), Wave attenuation by flexible, idealized salt marsh
615 vegetation, *Coastal Engineering*, *83*, 82–92.

- 616 Asano, T., H. Deguchi, and N. Kobayashi (1992), Interaction between water waves and
617 vegetation, in *Coastal Engineering Conference*, vol. 3, pp. 2710–2710, ASCE.
- 618 Augustin, L. N., J. L. Irish, and P. Lynett (2009), Laboratory and numerical studies of
619 wave damping by emergent and near-emergent wetland vegetation, *Coastal Engineering*,
620 *56*(3), 332–340.
- 621 Bradley, K., and C. Houser (2009), Relative velocity of seagrass blades: Implications for
622 wave attenuation in low-energy environments, *Journal of Geophysical Research: Earth*
623 *Surface*, *114*(F1).
- 624 Chen, S.-N., L. P. Sanford, E. W. Koch, F. Shi, and E. W. North (2007), A nearshore
625 model to investigate the effects of seagrass bed geometry on wave attenuation and
626 suspended sediment transport, *Estuaries and Coasts*, *30*(2), 296–310.
- 627 Coops, H., N. Geilen, H. J. Verheij, R. Boeters, and G. van der Velde (1996), Interactions
628 between waves, bank erosion and emergent vegetation: an experimental study in a wave
629 tank, *Aquatic Botany*, *53*(3), 187–198.
- 630 Dalrymple, R. A., J. T. Kirby, and P. A. Hwang (1984), Wave diffraction due to areas
631 of energy dissipation, *Journal of Waterway, Port, Coastal, and Ocean Engineering*,
632 *110*(1), 67–79.
- 633 Duarte, C. M. (1991), Seagrass depth limits, *Aquatic Botany*, *40*(4), 363–377.
- 634 Duarte, C. M., E. Benavent, and M. del Carmen Sánchez (1999), The microcosm of
635 particles within seagrass *Posidonia oceanica* canopies, *Marine Ecology Progress Series*,
636 *181*, 289–295.
- 637 Ellington, C. (1991), Aerodynamics and the origin of insect flight, *Advances in Insect*
638 *Physiology*, *23*, 171–210.

- 639 Elwany, M. H. S., W. C. O'Reilly, R. T. Guza, and R. E. Flick (1995), Effects of southern
640 california kelp beds on waves, *Journal of Waterway, Port, Coastal, and Ocean Engi-*
641 *neering*, 121(2), 143–150.
- 642 Eriander, L., E. Infantes, M. Olofsson, J. L. Olsen, and P.-O. Moksnes (2016), Assessing
643 methods for restoration of eelgrass (*Zostera marina* L.) in a cold temperate region,
644 *Journal of Experimental Marine Biology and Ecology*, 479, 76–88.
- 645 Fagherazzi, S., L. Carniello, L. D'Alpaos, and A. Defina (2006), Critical bifurcation of
646 shallow microtidal landforms in tidal flats and salt marshes, *Proceedings of the National*
647 *Academy of Sciences*, 103(22), 8337–8341.
- 648 Fonseca, M. S., and J. A. Cahalan (1992), A preliminary evaluation of wave attenuation
649 by four species of seagrass, *Estuarine, Coastal and Shelf Science*, 35(6), 565–576.
- 650 Fonseca, M. S., J. C. Zieman, G. W. Thayer, and J. S. Fisher (1983), The role of current
651 velocity in structuring eelgrass (*Zostera marina* L.) meadows, *Estuarine, Coastal and*
652 *Shelf Science*, 17(4), 367–380.
- 653 Gacia, E., T. Granata, and C. Duarte (1999), An approach to measurement of particle flux
654 and sediment retention within seagrass (*Posidonia oceanica*) meadows, *Aquatic Botany*,
655 65(1), 255–268.
- 656 Ghisalberti, M., and H. M. Nepf (2002), Mixing layers and coherent structures in vegetated
657 aquatic flows, *Journal of Geophysical Research: Oceans*, 107(C2).
- 658 Gijón Mancheño, A. (2016), Interaction between wave hydrodynamics and flexible vege-
659 tation, Master's thesis, TU Delft.
- 660 Gosselin, F., E. De Langre, and B. A. Machado-Almeida (2010), Drag reduction of flexible
661 plates by reconfiguration, *Journal of Fluid Mechanics*, 650, 319–341.

- 662 Graham, J. (1980), The forces on sharp-edged cylinders in oscillatory flow at low keulegan–
663 carpenter numbers, *Journal of Fluid Mechanics*, 97(02), 331–346.
- 664 Granata, T., T. Serra, J. Colomer, X. Casamitjana, C. Duarte, and E. Gacia (2001), Flow
665 and particle distributions in a nearshore seagrass meadow before and after a storm,
666 *Marine Ecology Progress Series*, 218, 95–106.
- 667 Hunt, J. (1964), The viscous damping of gravity waves in shallow water, *La Houille*
668 *Blanche*, 6, 685–691.
- 669 Infantes, E., A. Orfila, G. Simarro, J. Terrados, M. Luhar, and H. Nepf (2012), Effect of a
670 seagrass (*Posidonia oceanica*) meadow on wave propagation, *Marine Ecology Progress*
671 *Series*, 456, 63–72.
- 672 Keulegan, G. H., and L. H. Carpenter (1956), *Forces on cylinders and plates in an oscil-*
673 *lating fluid*, US Department of Commerce, National Bureau of Standards.
- 674 Knutson, P. L., R. A. Brochu, W. N. Seelig, and M. Inskeep (1982), Wave damping in
675 *Spartina alterniflora* marshes, *Wetlands*, 2(1), 87–104.
- 676 Kobayashi, N., A. W. Raichle, and T. Asano (1993), Wave attenuation by vegetation,
677 *Journal of Waterway, Port, Coastal, and Ocean Engineering*, 119(1), 30–48.
- 678 Koch, E. W., J. D. Ackerman, J. Verduin, and M. van Keulen (2006), Fluid dynamics
679 in seagrass ecology: from molecules to ecosystems, in *Seagrasses: Biology, Ecology and*
680 *Conservation*, pp. 193–225, Springer, Netherlands.
- 681 Lowe, R. J., J. L. Falter, J. R. Koseff, S. G. Monismith, and M. J. Atkinson (2007),
682 Spectral wave flow attenuation within submerged canopies: Implications for wave energy
683 dissipation, *Journal of Geophysical Research: Oceans*, 112(C5).

- 684 Luhar, M., and H. Nepf (2016), Wave-induced dynamics of flexible blades, *Journal of*
685 *Fluids and Structures*, *61*, 20–41.
- 686 Luhar, M., and H. M. Nepf (2011), Flow-induced reconfiguration of buoyant and flexible
687 aquatic vegetation, *Limnology and Oceanography*, *56*(6), 2003–2017.
- 688 Luhar, M., J. Rominger, and H. Nepf (2008), Interaction between flow, transport and
689 vegetation spatial structure, *Environmental Fluid Mechanics*, *8*(5-6), 423–439.
- 690 Luhar, M., S. Coutu, E. Infantes, S. Fox, and H. Nepf (2010), Wave-induced velocities
691 inside a model seagrass bed, *Journal of Geophysical Research: Oceans*, *115*(C12).
- 692 Luhar, M., E. Infantes, A. Orfila, J. Terrados, and H. M. Nepf (2013), Field observations
693 of wave-induced streaming through a submerged seagrass (*Posidonia oceanica*) meadow,
694 *Journal of Geophysical Research: Oceans*, *118*(4), 1955–1968.
- 695 Madsen, O. S. (1971), On the generation of long waves, *Journal of Geophysical Research*,
696 *76*(36), 8672–8683.
- 697 Marbà, N., C. M. Duarte, E. Díaz-Almela, J. Terrados, E. Álvarez, R. Martínez, R. San-
698 tiago, E. Gacia, and A. M. Grau (2005), Direct evidence of imbalanced seagrass (*Posi-*
699 *donia oceanica*) shoot population dynamics in the Spanish Mediterranean, *Estuaries*,
700 *28*(1), 53–62.
- 701 Méndez, F. J., and I. J. Losada (2004), An empirical model to estimate the propagation
702 of random breaking and nonbreaking waves over vegetation fields, *Coastal Engineering*,
703 *51*(2), 103–118.
- 704 Méndez, F. J., I. J. Losada, and M. A. Losada (1999), Hydrodynamics induced by wind
705 waves in a vegetation, *Journal of Geophysical Research*, *104*(C8), 18–383.

- 706 Möller, I., T. Spencer, J. French, D. Leggett, and M. Dixon (1999), Wave transformation
707 over salt marshes: a field and numerical modelling study from North Norfolk, England,
708 *Estuarine, Coastal and Shelf Science*, 49(3), 411–426.
- 709 Moore, K. A. (2004), Influence of seagrasses on water quality in shallow regions of the
710 lower Chesapeake Bay, *Journal of Coastal Research*, pp. 162–178.
- 711 Mork, M. (1996), The effect of kelp in wave damping, *Sarsia*, 80(4), 323–327.
- 712 Mullarney, J. C., and S. M. Henderson (2010), Wave-forced motion of submerged single-
713 stem vegetation, *Journal of Geophysical Research: Oceans*, 115(C12).
- 714 Paul, M., T. Bouma, and C. Amos (2012), Wave attenuation by submerged vegetation:
715 combining the effect of organism traits and tidal current, *Marine Ecology Progress*
716 *Series*, 444, 31–41.
- 717 Pergent-Martini, C., V. Rico-Raimondino, and G. Pergent (1994), Primary production of
718 *Posidonia oceanica* in the Mediterranean Basin, *Marine Biology*, 120(1), 9–15.
- 719 Peterson, C. H., R. A. Luettich Jr, F. Micheli, and G. A. Skilleter (2004), Attenuation
720 of water flow inside seagrass canopies of differing structure, *Marine Ecology Progress*
721 *Series*, 268, 81–92.
- 722 Riffe, K. C., S. M. Henderson, and J. C. Mullarney (2011), Wave dissipation by flexible
723 vegetation, *Geophysical Research Letters*, 38(18).
- 724 Sánchez-González, J. F., V. Sánchez-Rojas, and C. D. Memos (2011), Wave attenuation
725 due to *Posidonia oceanica* meadows, *Journal of Hydraulic Research*, 49(4), 503–514.
- 726 Stratigaki, V., E. Manca, P. Prinos, I. J. Losada, J. L. Lara, M. Sclavo, C. L. Amos,
727 I. Cáceres, and A. Sánchez-Arcilla (2011), Large-scale experiments on wave propagation
728 over *Posidonia oceanica*, *Journal of Hydraulic Research*, 49(sup1), 31–43.

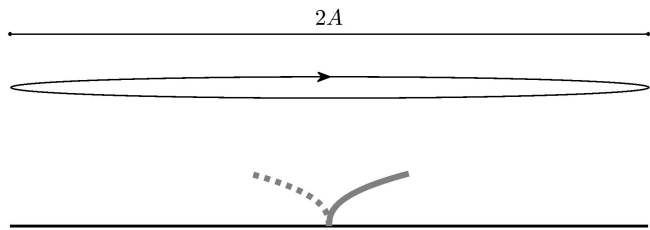
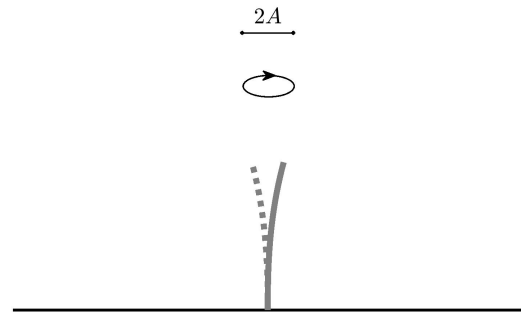
a) $L \ll 1$ b) $L \gg 1$ 

Figure 1. Schematic illustrating the difference in blade behavior at (a) the large excursion limit ($L \ll 1$) and (b) the small excursion limit ($L \gg 1$). This figure is modified from [Luhar and Nepf \[2016\]](#).

729 Vogel, S. (1994), *Life in moving fluids: the physical biology of flow*, Princeton University
 730 Press, New Jersey.

731 Ward, L. G., W. M. Kemp, and W. R. Boynton (1984), The influence of waves and
 732 seagrass communities on suspended particulates in an estuarine embayment, *Marine*
 733 *Geology*, 59(1-4), 85–103.

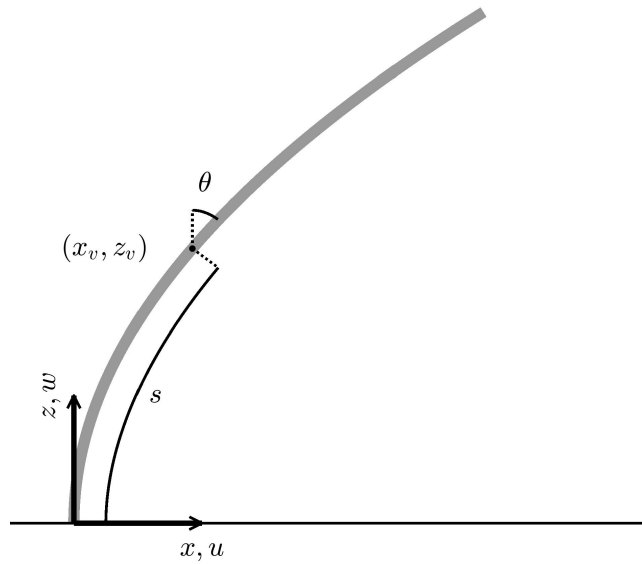


Figure 2. Schematic showing the coordinate system used to estimate blade posture, velocity and drag.

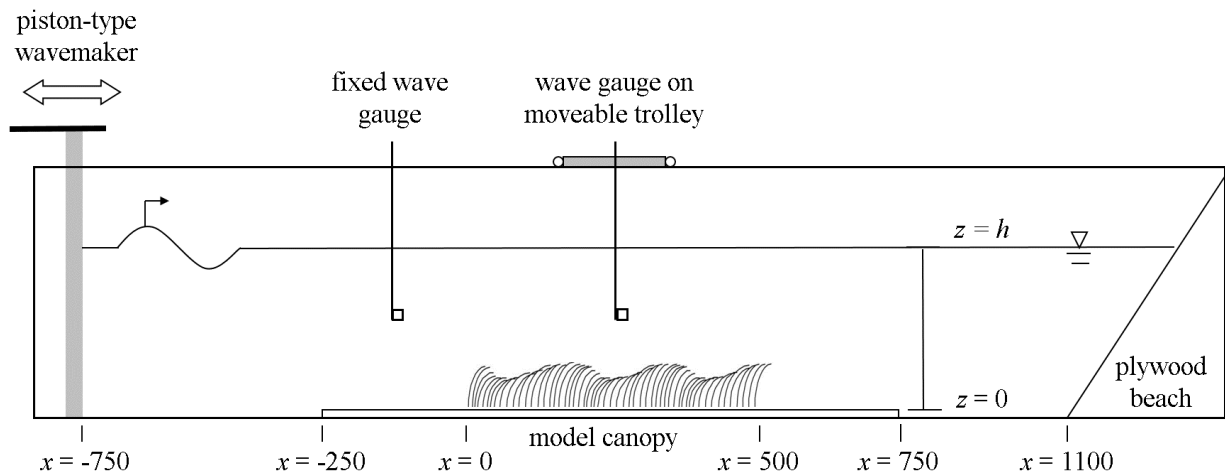


Figure 3. Schematic showing a side view of the wave channel (all dimensions cm; not to scale). The direction of wave propagation, as indicated by the arrow, is from left to right. Baseboards were put in place for the region 2.5m-upstream and 2.5m-downstream of the model seagrass canopy to ensure that any measured wave transformation was due to the vegetation alone. The slope of the plywood beach is 1:5.

Table 1. Table listing the wave and vegetation parameters for the experiments. Runs D1-D6 measure wave decay over a range of vegetation densities. Similarly, H1-H4 vary water depth, T1-T5 vary wave period while A1-A5 vary wave amplitude. The final row indicates typical uncertainty for each variable.

	n [m ⁻²]	h [cm]	T [s]	a_0 [cm]	λ [cm]	$a_v l$	l/h	kh	a_0/h	Re	KC	Ca	L	l_e/l
D1	1800	39	1.4	3.0	240	0.7	0.3	1.0	0.08	330	52	1030	5.3	-
D2	3600	39	1.4	3.3	240	1.4	0.3	1.0	0.09	360	58	1300	4.7	-
D3	5400	39	1.4	3.0	240	2.1	0.3	1.0	0.08	330	52	1050	5.2	-
D4 ^{*,+}	7200	39	1.4	3.4	240	2.8	0.3	1.0	0.09	370	59	1330	4.6	0.21
D5	9000	39	1.4	3.2	240	3.5	0.3	1.0	0.08	350	55	1180	4.9	-
D6	10800	39	1.4	2.8	240	4.2	0.3	1.0	0.07	310	49	910	5.6	-
H1	7200	16	1.4	1.4	170	2.8	0.8	0.6	0.09	290	47	850	5.8	-
H2	7200	24	1.4	2.0	210	2.8	0.5	0.7	0.08	330	53	1070	5.2	-
H3	7200	32	1.4	2.6	230	2.8	0.4	0.9	0.08	350	55	1170	4.9	-
H4 ^{*,+}	7200	39	1.4	3.4	240	2.8	0.3	1.0	0.09	370	59	1330	4.6	0.21
T1	7200	39	0.8	3.6	90	2.8	0.3	2.7	0.09	120	11	150	25.9	-
T2 [*]	7200	39	0.9	2.7	125	2.8	0.3	2.0	0.07	160	16	260	16.5	0.35
T3 [*]	7200	39	1.1	3.7	170	2.8	0.3	1.4	0.09	310	39	970	7.0	0.21
T4 ^{*,+}	7200	39	1.4	3.4	240	2.8	0.3	1.0	0.09	370	59	1330	4.6	0.21
T5 [*]	7200	39	2.0	3.5	370	2.8	0.3	0.7	0.09	460	102	2060	2.7	0.23
A1 [*]	7200	39	1.4	0.9	240	2.8	0.3	1.0	0.02	100	16	100	17.1	0.40
A2	7200	39	1.4	1.9	240	2.8	0.3	1.0	0.05	210	33	420	8.2	-
A3 ^{*,+}	7200	39	1.4	3.4	240	2.8	0.3	1.0	0.09	370	59	1330	4.6	0.21
A4	7200	39	1.4	4.8	240	2.8	0.3	1.0	0.12	530	84	2710	3.3	-
A5 [*]	7200	39	1.4	5.6	240	2.8	0.3	1.0	0.14	610	97	3610	2.8	0.20
	[30]	[0.5]	[0.05]	[0.2]	[5]									[0.03]

* Blade motion was tracked for these runs, yielding direct measurement of l_e via [15].

+ D4, H4, T4 and A3 are identical runs listed in multiple locations for ease of comparison.

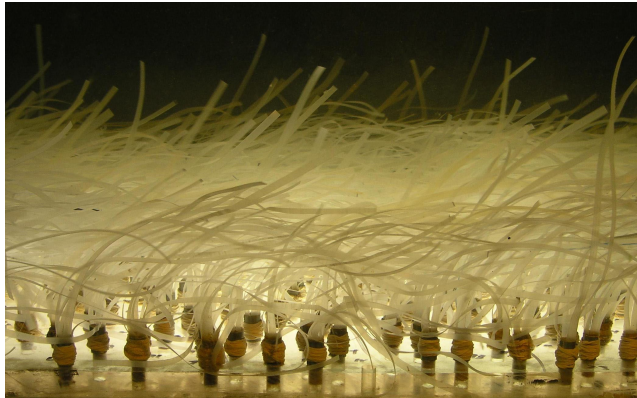


Figure 4. Photo of the model canopy with wave approaching from the left. The seagrass density is $1800 \text{ stems m}^{-2}$. The stem protrudes approximately 1 cm above the baseboards into the water. The mean measured diameter of the stems was $d = 7.8 \text{ mm}$.

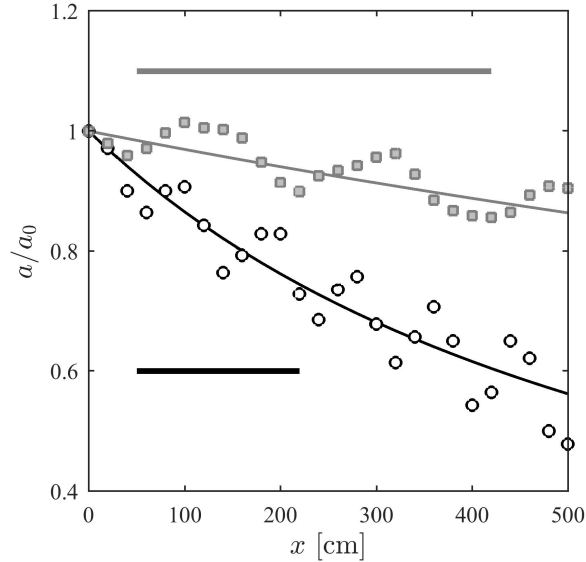


Figure 5. Wave amplitude measurements for runs H1 ($a_0 = 1.4$ cm, $T = 1.4$ s, $h = 16$ cm; open black circles) and T5 ($a_0 = 3.5$ cm, $T = 2.0$ s, $h = 39$ cm; filled gray squares). The best-fit decay curves for these measurements correspond to $K_D a_0 \lambda = 0.26$ for run H1 (fine black line) and $K_D a_0 \lambda = 0.12$ (fine gray line) for run T5. The heavy gray line shown above the measurements indicates the wavelength for run T5 ($\lambda = 370$ cm) and the heavy black line shown below the measurements indicates the wavelength for run H1 ($\lambda = 170$ cm). The oscillation in measured wave amplitudes reflects the partially standing wave created due to downstream reflection; as a result it is periodic with a spatial scale of $\lambda/2$.

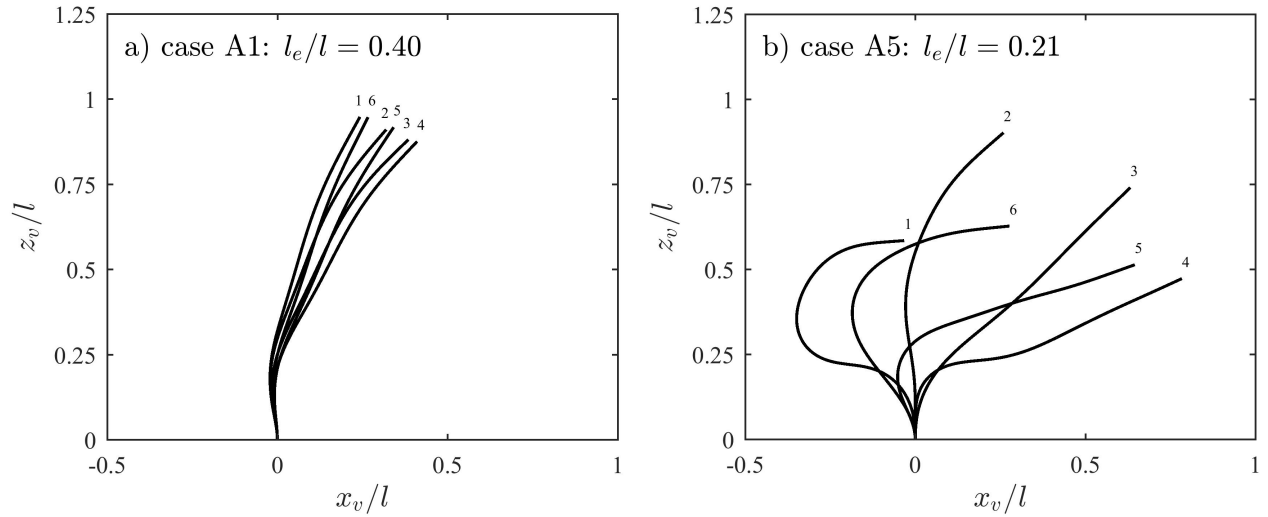


Figure 6. (a) Blade posture at six different phases during a cycle for wave conditions corresponding to case A1. Curves 1, 2 and 3 indicate blade posture during the passage of a wave crest while curves 4, 5 and 6 show posture under a wave trough. (b) Blade posture for wave conditions corresponding to case A5. Also shown on the plots is the estimated effective blade length l_e , calculated using [15]. [Movies of blade motion for cases A1 and A5 are included in Supplementary Information.](#)

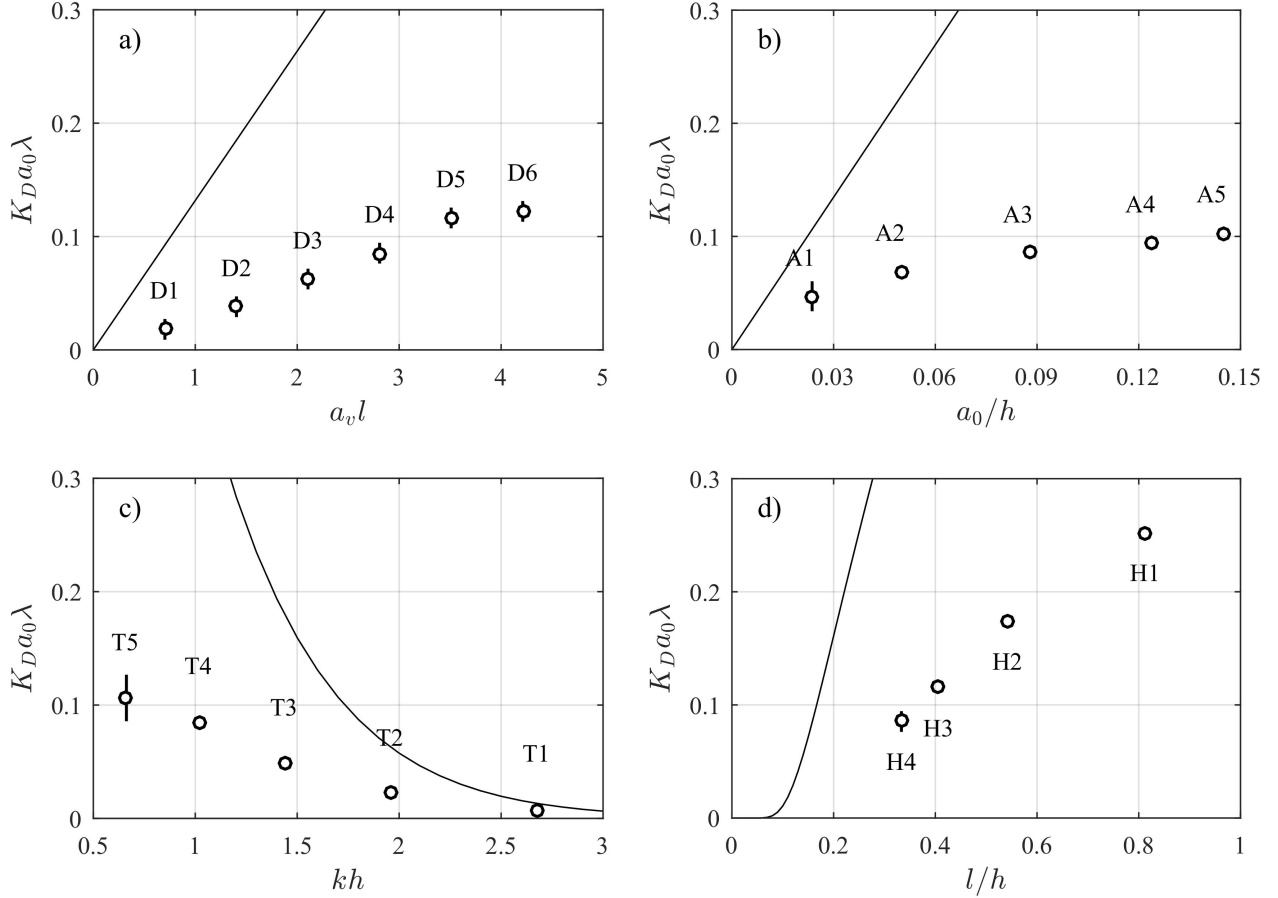


Figure 7. Measured wave decay per wavelength ($K_D a_0 \lambda$). (a) Experiments D1-D6: varying vegetation density, expressed as the dimensionless parameter $a_v l$, (b) experiments A1-A5: varying wave amplitude, plotted as a_0/h , (c) experiments T1-T5: varying wave period (and wavelength) expressed as kh , and (d) experiments H1-H4: varying water depth, plotted as l/h . For experiments D1-D6, A1-A5 and T1-T5, only one dimensionless parameter varies (e.g. for A1-A5, kh , l/h and $a_v l$ are constant). For experiments H1-H4, however, both a_0/h (0.3-0.8) and kh (0.6-1.0) vary. See Table 1 for more detail. The solid lines show predicted decay based on [8] assuming $C_D = 1.95$ and $l_e = l$. The error bars represent 95% confidence limits on the fitted wave decay parameter $K_D a_0 \lambda$. The major source of error in all cases was wave reflection from the downstream end of the flume.

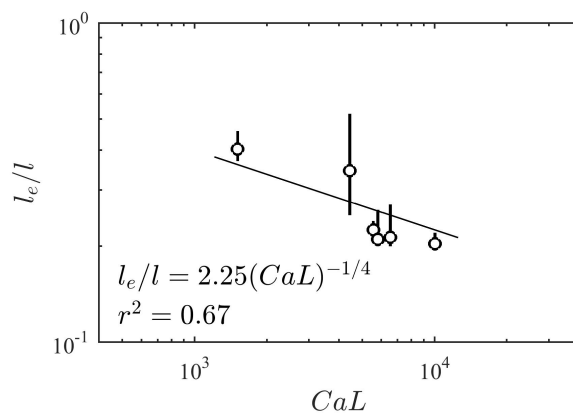


Figure 8. Estimated effective lengths from blade motion images l_e/l plotted against the product of the Cauchy number and the length ratio, CaL . The error bars reflect range of estimated effective lengths obtained by shifting the recorded blade motion by 1 phase bin (i.e. 1/15 of a second) relative to the linear wave velocity field. The line shows the best-fit power law with the exponent constrained to be $-1/4$.

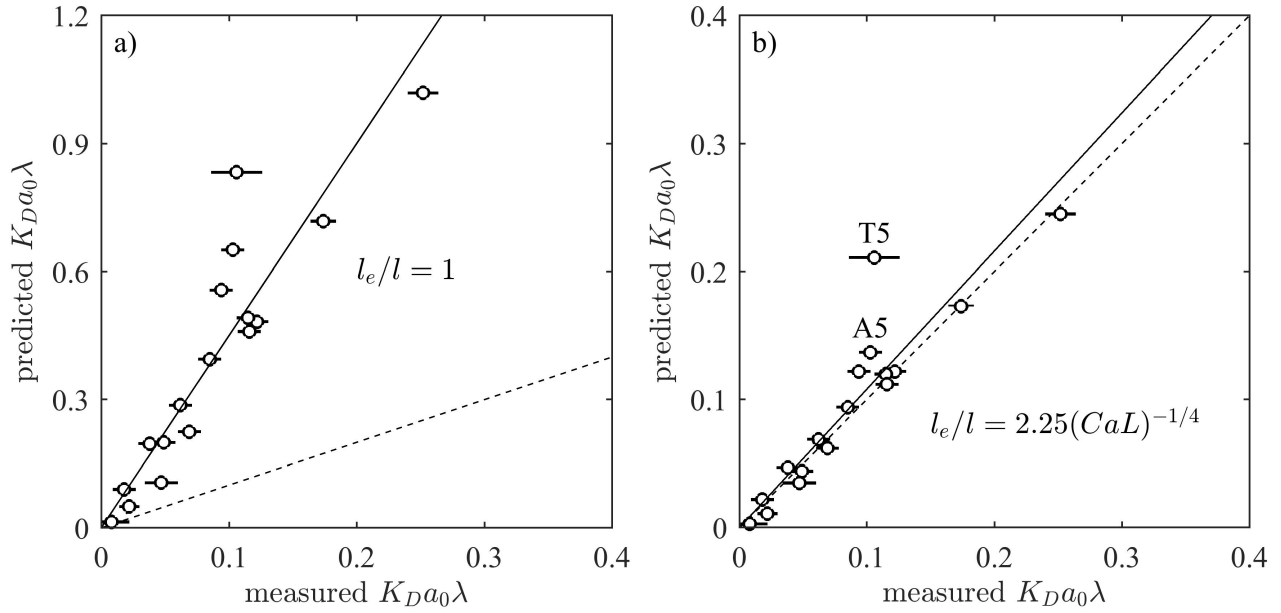


Figure 9. Measured and predicted wave decay for all the cases shown in Table 2. (a) Predictions assuming $l_e/l = 1$. (b) Predictions assuming $l_e/l = 2.25(CaL)^{-1/4}$, the best-fit power law from Figure 8. The solid lines show the best-fit linear relationships with zero intercept: the fitted slopes are 4.50 ($r^2 = 0.83$) for (a) and 1.08 ($r^2 = 0.84$) for (b). The dashed lines indicate perfect agreement.

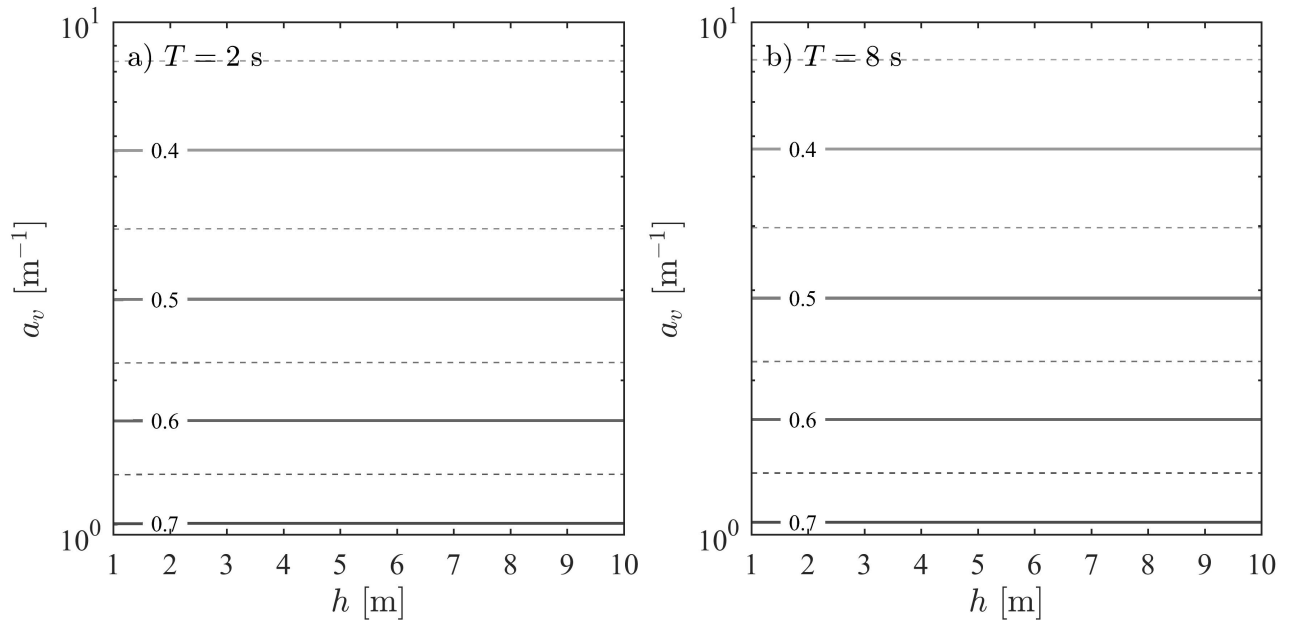


Figure 10. Contours showing ratio of steady-state wave amplitudes over vegetated and bare beds a_{veg}/a_{bf} as a function of vegetation frontal area density a_v and water depth h . (a) Amplitude ratio for waves of period $T = 2$ s. (b) Amplitude ratio for waves of period $T = 8$ s.